

# Piezoelectric Approach on Harvesting Acoustic Energy

Khin Fai Chen, Jee-Hou Ho, Eng Hwa Yap

**Abstract**—An Acoustic Micro-Energy Harvester (AMEH) is developed to convert wasted acoustical energy into useful electrical energy. AMEH is mathematically modeled using Lumped Element Modelling (LEM) and Euler-Bernoulli beam (EBB) modelling. An experiment is designed to validate the mathematical model and assess the feasibility of AMEH. Comparison of theoretical and experimental data on critical parameter value such as  $M_{mp}$ ,  $C_{ms}$ ,  $d_m$  and  $C_{eb}$  showed the variances are within 1% to 6%, which is reasonably acceptable. Then, AMEH undergoes bandwidth tuning for performance optimization. The AMEH successfully produces  $0.9V/(m/s^2)$  and  $1.79\mu W/(m^2/s^4)$  at 60Hz and  $400k\Omega$  resistive load which only show variances about 7% compared to theoretical data. At 1g and 60Hz resonance frequency, the averaged power output is about 2.2mW which fulfilled a range of wireless sensors and communication peripherals power requirements. Finally, the design for AMEH is assessed, validated and deemed as a feasible design.

**Keywords**—Piezoelectric, acoustic, energy harvester, thermoacoustic.

## I. INTRODUCTION

THE past few decades have witnessed the advancement and intensive utilization of wireless sensors and high technology electronics in human daily life, for instance, cell phone, mobile computers, sensory monitoring system, pacemakers and cardioverter-defibrillator. All these modern technologies stated above had two common characteristics: it needs battery and the battery will be depleted one day.

Battery technologies have remained stagnant compared to computing and electronics technology where it no longer able to cope with the ever shrinking geometrical constraint and increasing power density requirements [1]. Providing a better battery solution is achievable through new battery composition and design, but even every new battery design could deplete one day, needless to mention the cost and reliability of the new battery technology. Therefore, a more comprehensive and ultimate solution is needed i.e. battery elimination. It is possible by implementing a self-sustaining energy source where the energy originates from the ambient environment through energy harvesting [2].

In this research paper, the ambient environment would revolve around a SCORE stove. SCORE stands for Stove for Cooking, Refrigeration and Electricity. It combines the functionalities of a high efficiency cooking stove, an electricity generator and fuelled by biomass products such as

Chen Khin Fai is an academic lecturer and active researcher in University of Nottingham Malaysia Campus (UNMC) where he is attached with Energy, Power and Fuel Technology Division. UNMC, Jln. Broga, 43500 Semenyih, Malaysia (+603-87233554; e-mail: khinfai.chen@nottingham.edu.my).

Ho Jee Hou is an Associate Professor with University of Nottingham Malaysia Campus (UNMC) (e-mail: jeehou.ho@nottingham.edu.my).

Yap Eng Hwa is a Senior Lecturer with University College London (UCL) School of Energy and Resources (e-mail: e.yap@ucl.ac.uk).

wood. The waste heat is used to power a thermoacoustic engine and generates power by using a loudspeaker as a linear alternator. This innovation is simple, cheap, reliable and it uses of the wasted heat and the design output is expected to be used in poor or rural communities. Its working principle is based on the fact that a properly dimensioned tube that is heated at one end and has a porous heat absorbing substance separating it from the cooler end of the tube will generate sound. And it works both ways, feeding sound into the same tube will heat up one end of the tube to and the other cooled down. Researchers used heat to generate sound and the other using sound to pump heat out of a small fridge with a modify loudspeaker or generator between the two [3]. However, the sound generated is being “discharged” at the end of the process, which is a kind of wasted energy. Hence, the objective will be harvesting these wasted acoustical energy and convert it into useful electrical energy via piezoelectric approach.

## II. LITERATURE REVIEW

Piezoelectric materials are applied in many autonomous microsystem devices that designed to convert ambient mechanical energy into useful electrical energy. Most of the designs are based on mechanical resonant device that is targeted to match the vibration spectrum of the source and based on forced, damped harmonic oscillator. A few common configurations for piezoelectric device are cantilever and diaphragm. In fact, there are too many devices available in the literature search and those, which had revelation with acoustic energy harvesting and piezoelectric, will be highlighted here.

Acoustic noise is a product from pressure waves, which is a resultant of vibration. A few examples of acoustic noise are acoustic power and acoustic pressure. Acoustic power is the total amount of sound energy radiated in a time frame and expressed in Watts. Acoustic pressure is a reference of hearing threshold of human ear, which is 20dB [4].

A team of researcher from University of Florida fabricated two devices in millimeters scale and incorporates a Helmholtz resonator. The piezoelectric material used is PZT-based custom fabricated and operated in diaphragm mode. The resonant frequencies measured are 12.6 kHz and 5.2 kHz. The output is connected to a linear regulator and an AC to DC flyback converter to increase the power transfer from the piezoelectric patch to the storage medium and also allows the circuit impedance to be matched with the impedance of the piezoelectric device. Results showed that the maximum power density harvested was around  $0.34\mu Wcm^{-2}$  at 149 dB, posting an efficiency of 0.0012% only. Further investigation shows that the sources of unacceptable low efficiency are PZT material quality, poling capability and residual stress, where if

all of the issues are addressed, the output power density would be in the order of  $250\mu\text{Wcm}^{-2}$  and overall efficiency would be 8.8% [5]. Later, the device technology is improvised by adjusting the resonator acoustic impedance and additional degree of freedom added by coupling it to a passive electrical shunt network. Experiment shows that the device able to produce 20-30mW continuous power at 151dB. The device is later incorporated for the development of self-powered, wireless, active acoustic liner system in aeroacoustics [6]. The work is continued by another team of researchers where results show approximately 30mW of output power is harvested for an incident sound pressure level of 160 dB with fly back converter. Such power is suffice whole wide range of low power electronic devices [7].

Researchers investigated acoustical energy harvesting using piezoelectric curved beams in the cavity of a sonic crystal [8]. The piezoelectric beam is located in the cavity of the sonic crystal. The sonic crystal is used to localize the acoustic wave as the acoustic wave is incident into the sonic crystal at the resonant frequency. Energy harvesting is achieved as the acoustic waves are incident at the resonant frequency. The piezoelectric material used is PVDF. The resonant frequency of the sonic crystal is 4.21 kHz. Using a speaker to generate acoustic pressure, the frequency is matched with the sonic crystal resonant frequency. It is also found out that the acoustic wave is a sinusoidal function of time, which mean external force applied on the PVDF film is harmonic at frequency 4.21 kHz. The maximum measured output voltage and power is 26 mV and 37 nW respectively, both at load resistance of 16 k $\Omega$ .

### III. MATHEMATICAL MODELLING

Euler-Bernoulli Beam (EBB) modelling is used to model AMEH. Fig. 1 shows a simple schematic diagram of a PZT composite beam energy harvester developed with base excitation. Supposedly the whole system is in an accelerating frame of reference under excitation frequency,  $f_{ext}$  of the base excitation. EBB provides an analytical solution to characterize deflected beam behavior under loading.

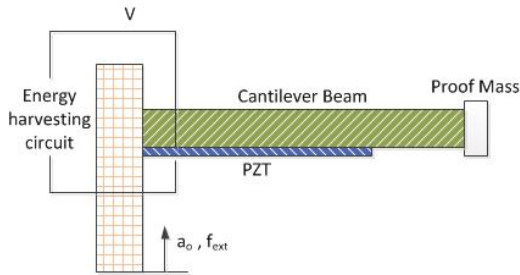


Fig. 1 Simple schematic diagram of a PZT composite beam energy harvester

Fig. 2 shows an equivalent electromechanical circuit that represents the PZT cantilever beam from Fig. 1. The circuit is drafted by lumping the distributed energy stored and dissipated in the system into simple circuit elements. First

subscript  $m$  represents mechanical domain and  $e$  represents electrical domain. Second subscript  $s$  and  $b$  represents short circuit and blocked, respectively. Effective force,  $F$  is a product of input acceleration and effective tip mass is applied to the structure which resulted in tip velocity;  $U$ .  $V$  and  $I$  represent voltage and current generated respectively.

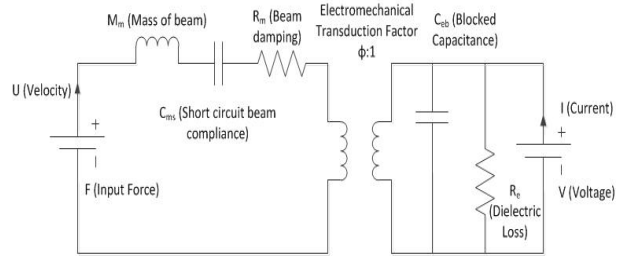


Fig. 2 PZT cantilever beam represented by an equivalent electromechanical circuit

PZT cantilever beam is analyzed for all the static mechanical loads acting on it from first principles using linear Euler-Bernoulli beam theory. The shear and rotary inertia effects are neglected. The clamp structure is replaced with bending moment,  $M_r$  and reaction force,  $R$ . A free body diagram is presented at Fig. 3.

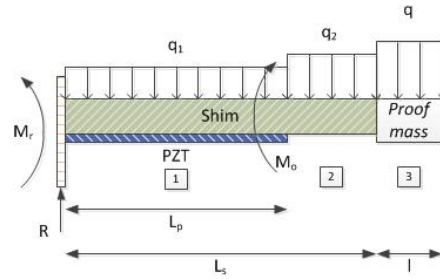


Fig. 3 Free body diagram of the static electromechanical model

The mass of the beam is replaced as equivalent uniform load due to its weight and can be represented with an effective static load density:

$$q = \rho_m whg \quad (1)$$

$$q_1 = (\rho_s t_s b_s + \rho_p t_p b_p)g \quad (2)$$

$$q_2 = \rho_s t_s b_s g \quad (3)$$

$q$ ,  $q_1$  and  $q_2$  are load densities (N/m).  $w$  and  $h$  is the width and thickness of the proof mass.  $\rho$ ,  $t$  and  $b$  is density, thickness and width respectively. Subscripts  $m$ ,  $s$  and  $p$  represent proof mass, shim and PZT respectively. Assuming the beam is in static equilibrium, expression for the bending moment and reaction force can be obtained:

$$R = q_1 L_p + q_2 (L_s - L_p) + ql \quad (4)$$

$$M_r = - \left[ q_1 \frac{L_p^2}{2} + q_2 \frac{L_s^2 - L_p^2}{2} + ql \left( L_s + \frac{l}{2} \right) \right] \quad (5)$$

The composite beam is now divided into three different sections. First section consists of the composite where  $0 \leq x \leq L_p$ . Second section consists of the shim where  $L_p \leq x \leq L_s$ . Third section consists proof mass where  $L_s \leq x \leq L_s + l$ . In order to obtain Euler-Bernoulli equation, bending moment and shear force for each section is obtained. Then, the bending moment is integrated to obtain the mode shape.

Each section had their respective flexural rigidity, namely  $(EI)_c$ ,  $(EI)_s$  and  $(EI)_m$  respectively where  $E$  is the elastic modulus and  $I$  is the moment of inertia. Transverse deflection in each section at a distance  $x$  from the clamp is represented as  $w_1(x)$ ,  $w_2(x)$  and  $w_3(x)$ . Boundary condition can be obtained from clamped boundary condition and deflection and slope matching of each section interfaces. Finally, the Euler-Bernoulli equation is solved and represented as:

$$w_1(x) = \frac{q_1 x^4}{24(EI)_c} + \frac{[q_1 L_p + q_2(L_s - L_p) + ql]x^3}{6(EI)_c} - \frac{\left[ q_1 \left( \frac{L_p^2}{2} \right) + q_2 l \left( \frac{L_s^2 - L_p^2}{2} \right) + ql \left( L_s + \frac{l}{2} \right) + M_o \right] x^2}{2(EI)_c} \quad (6)$$

$$w_2(x) = -\frac{q_2 x^4}{24(EI)_s} + \frac{(q_2 L_s + ql)x^3}{6(EI)_s} - \frac{\left[ q_2 \left( \frac{L_s^2}{2} \right) + ql \left( L_s + \frac{l}{2} \right) \right] x^2}{2(EI)_s} + \frac{(C_1 + C_3)x}{(EI)_s} + \frac{C_2 + C_4}{(EI)_s} \quad (7)$$

$$w_3(x) = -\frac{q_2 x^4}{24(EI)_m} + \frac{q(L_s + l)x^3}{6(EI)_m} - \frac{q(L_s + l)^2 x^2}{4(EI)_m} + \frac{(C_5 + C_7)x}{(EI)_m} + \frac{C_6 + C_8}{(EI)_m} \quad (8)$$

where:

$$C_1 = \frac{L_p}{6} \left[ L_p^2 (q_2 - q_1 \alpha) + 3q_2 L_s (L_s - L_p) (1 - \alpha) \right] \quad (9)$$

$$C_2 = \frac{L_p^2}{24} \left[ L_p^2 (q_1 \alpha - q_2 (3 - 2\alpha)) + q_2 L_s (8L_p - 6L_s) (1 - \alpha) \right] \quad (10)$$

$$C_3 = \frac{L_p}{2} \left[ ql(1 - \alpha)(2L_s - L_p + l) - 2\alpha M_o \right] \quad (11)$$

$$C_4 = L_p^2 \left[ \frac{M_o \alpha}{2} + ql(1 - \alpha) \left( \frac{L_p}{3} - \frac{l}{4} - \frac{L_s}{2} \right) \right] \quad (12)$$

$$C_5 = \gamma \left[ C_1 - \frac{q_2 L_s^3}{6} \right] \quad (13)$$

$$C_6 = \gamma \left[ C_2 - \frac{q_2 L_s^4}{24} \right] \quad (14)$$

$$C_7 = C_3 \gamma + \frac{qL_s^3}{6} + \frac{1}{2} qL_s (L_s - l) (1 - \gamma) \quad (15)$$

$$C_8 = C_4 \gamma - \frac{1}{24} [qL_s^4 + qlL_s^2 (1 - \gamma) (4L_s + 6l)] \quad (16)$$

where  $\alpha = (EI)_s / (EI)_c$  and  $\gamma = (EI)_m / (EI)_s$ . Equations (6) to (16) is an analytical solution of all parameters and useful for optimization the structure for maximum power output. Static deflection mode shape can now be used to obtain equivalent mass and compliance for simplification purposes. In this case, only mechanical load is considered. Based on this assumption, the equivalent electromechanical circuit in Fig. 2 is simplified where the electrical side is eliminated, leading to a short circuit electrical condition for the PZT. Stored potential energy (PE) and kinetic energy (KE) associated with distributed strain energy for the PZT beam is:

$$PE = \sum_1^3 \frac{EI}{2} \int_0^L \left( \frac{d^2 w(x)}{dx^2} \right)^2 dx \quad (17)$$

$$KE = \sum_1^3 \frac{\rho_L}{2} \int_0^L \dot{w}(x)^2 dx \quad (18)$$

where  $\rho_L$  is the ratio of mass over length of the section and  $\dot{w}(x)$  is the velocity of the section. Lumping the overall potential strain energy at the tip produce short circuit mechanical compliance and mass for the PZT:

$$C_{ms} = \frac{(w_{tip,F})^2}{2PE} \quad (19)$$

$$M_m = \frac{2KE}{(w_{tip,F})^2} \quad (20)$$

where  $w_{tip,F} = w_3(L_s + l)$  is the resulting tip deflection of the beam due to self-weight. The natural frequency of the composite beam can be obtained from the effective mass and compliance expression:

$$f_n = \frac{1}{2\pi} \sqrt{\frac{1}{C_{ms} M_m}} \quad (21)$$

To obtain the effective piezoelectric coefficient, which is the tip deflection due to converse piezoelectric effect, all mechanical loads term is eliminated and effect of voltage on the deflection can be decoupled from the overall equations and therefore given by:

$$d_m = \frac{w_{tip,v}}{V_{app}} = -\frac{d_{31} E_p b_p (2c_2 - t_p) L_p}{2(EI)_c} \left( L_s - \frac{L_p}{2} \right) \quad (22)$$

From Fig. 2, the transduction factor  $\phi$  is defined as the turn's ratio for the transformation between electrical and mechanical domains, which is given by:

$$\phi = -\frac{d_m}{C_{ms}} \quad (23)$$

Blocked electrical capacitance is given by:

$$C_{eb} = C_{ef} (1 - \kappa^2) \quad (24)$$

where  $C_{ef}$  is the free electrical capacitance and  $\kappa^2$  is the electromechanical coupling coefficient, and it's given by:

$$C_{ef} = \frac{\epsilon A_p}{t_p} \quad (25)$$

$$\kappa^2 = \frac{d_m^2}{C_{ef} C_{ms}} \quad (26)$$

Resistive elements in the circuit are given by:

$$R_m = 2\zeta \sqrt{\frac{M_m}{C_{ms}}} \quad (27)$$

$$R_e = \frac{1}{\tan \delta (2\pi f_n C_{eb})} \quad (28)$$

From Fig. 1, it can be seen that the whole system was under acceleration due to base excitation and the equivalent force is

given by:

$$F = M_m a_o + M_m g \quad (29)$$

From (29), the first term is the input force due to base excitation acceleration and the second term is the beam static deflection due to gravity. The beam is connected to energy harvesting circuit which has electrical impedance that determines the amount of harvested power. It is assumed that the energy harvesting circuit is purely resistive, where it is simplified to a Thévenin equivalent circuit, as shown in Fig. 4.

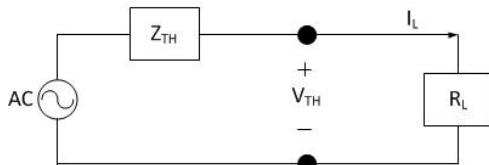


Fig. 4 Energy harvesting circuit represented as Thévenin equivalent circuit

Current across the load can be obtained using Ohm's Law:

$$I_L = \frac{V_{TH}}{Z_{TH} + R_L} \quad (30)$$

RMS power across the load is obtained as:

$$P_{L,rms} = \frac{1}{2} |I_L|^2 R_L \quad (31)$$

Input power to the device can be calculated using:

$$P_{in} = \frac{1}{2} |F||U| \quad (32)$$

Efficiency of the power transfer is the ratio of (31) and (32):

$$\eta = \frac{P_{L,rms}}{P_{in}} = \frac{|I_L|^2 R_L}{|F||U|} \quad (33)$$

#### IV. DESIGN OF EXPERIMENT

Due to the unavailability of SCORE stove at the point of experimental work, the frequency generated will be replicated. There are three auxiliary parts that need to be prepared. First, PZT clamp which is used to clamp the PZT cantilever bimorph securely need to be properly designed and fabricated because insecure placement will produce significant errors in data trend. Second is the configuration of buck boost circuitry. Third is the bandwidth tuning of the AMEH using tungsten mass. SCORE stove operate optimally at 60Hz. For performance optimization, PZT cantilever beam natural frequency is tuned to match the vibrating source.

Fig. 5 shows the designed experimental configuration for validation purposes. The electromagnetic shaker is used to replicate the ambient environment of the thermoacoustic engine by providing base acceleration of the acoustic wave. Displacement sensor is used to measure the tip deflection of the bimorph. Spectrum analyzer is used to measure the input acceleration of the whole structure. An oscilloscope is used to display the voltage and the beam vibrating frequency at a

frequency range. The electromagnetic shaker gives control on vibrating frequency and external excitation to AMEH. Multimeter is used for quantitative measurements of the current and voltage for the system. The resistive load is a resistance manipulator.

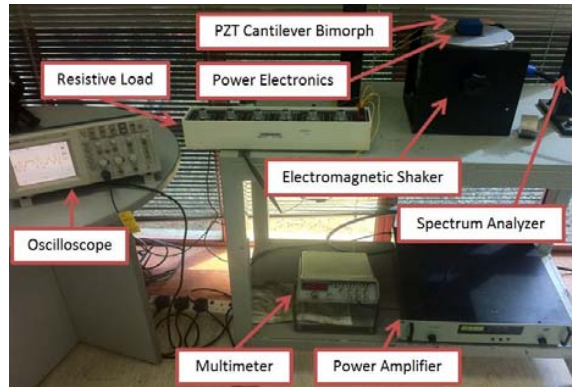


Fig. 5 Experiment configuration for validation purposes



Fig. 6 Buck boost circuitry as power electronics circuit

Power electronics are the buck boost circuitry as shown in Fig. 6. It consists of a low-loss full wave rectifier with a high efficiency Buck converter and integrated DC-DC conversion for high output impedance energy sources such as piezoelectric transducers. The DC output can be configured to 1.8V, 2.5V, 3.3V or 3.6V. The board also includes a 200μF of storage capacitance. It can provide up to 100mA of continuous output current.

The most effective means for vibration measurement is using accelerometer and perform Fast Fourier Transform (FTT) onto the data to quantify the frequency. SCORE stove operate optimally at 60Hz. For performance optimization, PZT cantilever beam natural frequency is tuned to match the source resonance frequency by attaching tungsten mass onto the tip of the bimorph until the natural frequency of the bimorph matched the source resonance frequency.

The easiest way for bandwidth tuning is to measure the frequency at which the device "decay" when excited by an impulse mechanical load. First, mount AMEH rigidly on a surface. Then the output is wired to an oscilloscope for monitoring and data acquisition. Add the tungsten mass incrementally and then apply an impulse mechanical load by lightly flicking the tip of the bimorph. The frequency of the decaying wave is the natural frequency of the tuned bimorph. Trial and error until the desired frequency is achieved by adding or reducing mass and changing location of the mass within the vicinity of the bimorph tip. During trial runs, bee's wax is used for non-permanent attachment during the tuning.

After the tuning is achieved, robust adhesive such as Loctite™ 404 is used on tungsten mass for permanent adhesion.

## V. RESULTS

In order to obtain the analytical results, it is important to apprehend all the required data and parameters for all the variables from (1) to (8). The geometrical data are obtained from precision measurement of the PZT cantilever bimorph. The density data of the bimorph are taken from a general value due to lack of information available from the manufacturer. Table I shows all the value for the data and parameters required.

TABLE I  
DATA AND PARAMETERS REQUIRED FOR ANALYTICAL SOLUTION

Parameters	Values
$w, b_s, b_p$	0.0381 m
$w_m$	0.0127 m
$L_s, L_p$	0.0459 m
$L_m$	$6.35 \times 10^{-3}$ m
$t_s, t_p$	0.0003 m
$t_m$	$2.54 \times 10^{-3}$ m
$\rho_m$	19250 kg/m <sup>3</sup>
$\rho_s$	1430 kg/m <sup>3</sup>
$\rho_p$	7800 kg/m <sup>3</sup>

Note that the Young's Modulus and 2<sup>nd</sup> moment of inertia values for all the masses were calculated based on general data. In order to validate the lumped element parameters, several tests were performed. Static tests were carried out by loading a tip mass and the tip deflection was measured using a laser displacement sensors. The average compliance of the composite beam can be calculated based on the ration of resulting tip deflection and the tip static load for all the masses. Then, an impulse test was done to obtain the natural frequency of the specimen. From the measured natural frequency and effective compliance, the effective mass can be calculated. On the other hand, a low frequency response value can be obtained by applying electric current onto the specimen where the tip motion was measured as a function of applied voltage. The value obtained from this electrical actuated response is approximated as the effective piezoelectric constant. Table II shows the comparison data from the theoretical analytical solution and experimental solution.

TABLE II  
COMPARISON DATA FOR THEORETICAL AND EXPERIMENTAL VALUE OF A PIEZOELECTRIC BIMOPRH

Parameters	Theoretical	Experimental	Variance
$M_m$	0.2114 g	0.2089 g	1.1 %
$C_{ms}$	0.0574m/N	0.0609m/N	5.7 %
$f_n$	120.43 Hz	118.92 Hz	1.3%
$d_m$	$-1.89 \times 10^{-6}$ m/V	$-2.12 \times 10^{-6}$ m/V	1.1%
$C_{ef}$	6.04 nF	5.86 nF	2.9 %
$C_{eb}$	5.94 nF	5.67nF	4.5%

Data obtained from the experimental works includes multiple response functions such as short circuit mechanical response, actuator response and open circuit voltage response.

These response functions were measured and compared with the analytical solution. From Table II, the variances of theoretical and experimental values are found out to be within 1% to 6%, which is reasonably acceptable. Since the lumped element parameters were verified, the AMEH mathematical model is now validated.

In order to optimize the performance of the harvester, the bimorph is tuned to match the operating frequency of the thermoacoustic engine, which is at 60Hz. From Table II, it is found out that the natural frequency of the harvester is 120Hz. Tip mass is applied to the tip of the bimorph with increment of 0.5grams and amplitude of 1g. The results are shown in Fig. 7 where. 4.5grams of tungsten mass is used.

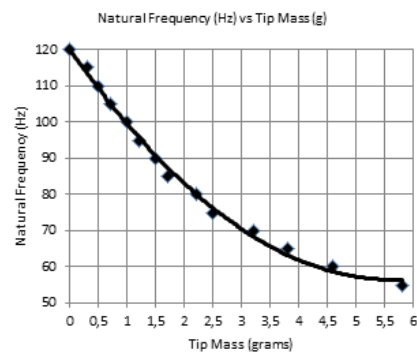


Fig. 7 Results from bandwidth tuning for the PZT cantilever bimorph using tungsten mass

After the lumped element model is verified, an input sinusoidal acceleration of  $1 \text{ m/s}^2$  RMS is applied at resonance frequency 60Hz. The resulting output voltages were measured across a range of resistive loads from  $10 \text{ k}\Omega$  to  $1 \text{ M}\Omega$  to measure the output power. Results for the measured RMS voltage are shown in Fig. 8.

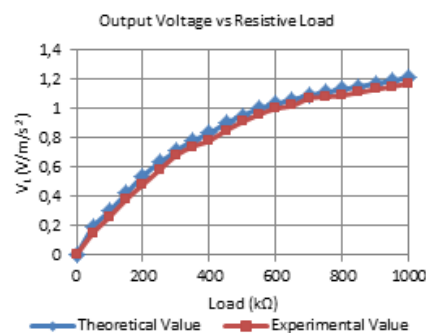


Fig. 8 Theoretical and experimental data comparison for voltage output per unit acceleration across various load resistance

From Fig. 8, it can be seen that the voltage output increases steadily until it begins to saturate to a constant value as the load increases. At 60Hz excitation, the harvester tip is suppressed as the resistive load is increased up to certain value, which leading to motion attenuation and then amplified. Since only open circuit voltage is only concerned, thus it can be seen that the output voltage increases in tandem with the

resistive load [9]. The constant value is deemed as open circuit voltage. It also shows that, the output voltage compared with the experimental values, it is normalized with the input acceleration.

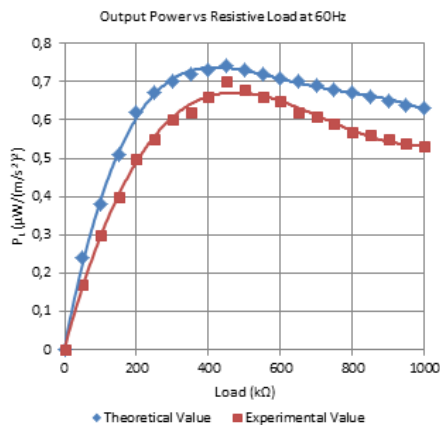


Fig. 9 Output power across resistive load at resonance frequency 60Hz

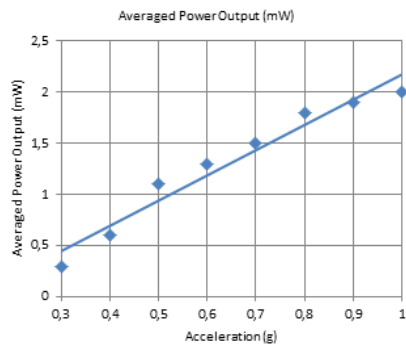


Fig. 10 Average power output ( $\mu\text{W}$ ) across series of acceleration (g)

Fig. 9 shows the output power per unit acceleration generated by AMEH across the resistive load at resonance frequency of 60Hz with an input sinusoidal acceleration of  $1\text{m/s}^2$  RMS. The figure also shows that the maximum power output is at optimal load of  $450\text{k}\Omega$ , which is close to the theoretical value of  $440\text{k}\Omega$ . Therefore, the output power is at maximum at an optimal resistance which happens when it is equal to the input impedance of AMEH. Table III shows the results comparison based on theoretical and experimental works for the voltage and power output at optimal load. The experimental data values are within 7% vicinity of theoretical values. The results obtained are reasonably agreed and acceptably small for design purposes.

TABLE III  
THEORETICAL AND EXPERIMENTAL DATA COMPARISON ON OPTIMAL LOAD AND VOLTAGE AND POWER OUTPUT

Parameters	Theoretical	Experimental
Optimal Load	$440\text{k}\Omega$	$450\text{k}\Omega$
Output voltage per unit acceleration	$0.9\text{V}/(\text{m}/\text{s}^2)$	$0.84\text{V}/(\text{m}/\text{s}^2)$
Output power per unit acceleration	$1.79\mu\text{W}/(\text{m}^2/\text{s}^4)$	$1.73\mu\text{W}/(\text{m}^2/\text{s}^4)$

At  $1\text{g}$ , 60Hz resonance frequency and  $200\mu\text{F}$  capacitor, the measured results for the average power output across a series of input acceleration is plotted. From Fig. 10, it can be seen that based on the pre-set boundary conditions,  $2.2\text{mW}$  of average power output can be harvested. AMEH managed to harvest  $2.2\text{mW}$  of electrical power.

## VI. DISCUSSIONS

The discrepancy of experimental results can be attributed to several reasons such as such assumption made for general parameter value of the PZT cantilever bimorph could be inaccurate. Then, utilizing EBB modelling had also ignored two factors, which is backward coupling and contributions from other vibration modes. In some cases, the backward coupling is assumed to be viscous damping [10], [11]. Such assumption is unsuitable because it will affect the variation of the natural frequencies rather than attenuation of motion amplitude [12]. The issue of backward coupling is addressed in DPM modelling, however it is not being applied here due to its complexity.

Final results showed that at  $1\text{g}$ , 60Hz and  $200\mu\text{F}$  capacitor, the average power output is  $2.2\text{mW}$ . After the analyses on data obtained, it is found that there are several ways to improve the power output. It is found out that AMEH installation site which the acoustic wave bombarded is about  $113\text{cm}^2$  whilst AMEH itself is only  $32\text{cm}^2$ . By optimized the geometrical factor of AMEH to fully utilize the bombardment site, the order of the power output harvested would be multiplied.

The piezoelectric material used for AMEH is a typical PZT5H. Using material with higher electromechanical coupling constant and Q factor would improve the harvested power density [2]. There are also many materials that combined two different attributes in a single material. For instance, magnetoelastic composites combine piezoelectric and magnetostrictive phases in one material and thus improve the efficiency of vibration energy harvesting.

In practice, the thermoacoustic engine will have a fluctuation of base excitation or input acceleration within its operation. AMEH is tuned specifically to perform optimally at the harvesting site resonance frequency. However, subjecting AMEH for other harvesting site with different frequency will render the device useless. Thus, it would be an ideal solution if AMEH is able to self-tune in virtually any vibration environment. Based on the nonlinearity of piezoelectric material, resonance is affected by the applied electrical voltage due to change of stiffness. As the applied voltage increases, resonance frequency will decrease [13]. Thus theoretically, the shift in operating frequency can be achieved through the bias voltage or stress.

Based on Table IV, it can be seen that the AMEH managed to fulfil a range of power devices from wireless sensors up to communication peripherals. Whilst SCORE only contained a range of wireless sensors node, AMEH can easily fulfilled the requirements to power up the entire wireless sensory networks.

TABLE IV  
POWER REQUIREMENTS FOR A RANGE OF ELECTRONIC APPLIANCES [14], [15]

Appliances	Power Requirements
Microcontroller, Wireless Sensors	1 $\mu$ W
RFID Tags	10 $\mu$ W
Implantable Cardiac Defibrillator	100 $\mu$ W
Hearing Aids	1mW
Bluetooth Communication	2.5mW
Radio Chipset	10mW
iPod Nano	100's mW
CPU Board, iPhone 5	1's W
MacBook Air	10's W

## VII. CONCLUSION

All the theoretical values are based on EBB Modelling. EBB Modelling is then verified based on certain critical parameter value such as  $M_m$ ,  $C_{ms}$ ,  $d_m$  and  $C_{eb}$ . Theoretical and experimental values are then compared and the variances are found out to be within 1% to 6%, which is reasonably acceptable. After the model validation, AMEH is tuned to match the resonance frequency, 60Hz using tungsten mass. The experimental data are compared with theoretical solution and the variances are found out to be within 7%. AMEH successfully produces 0.9 V/(m/s<sup>2</sup>) and 1.79  $\mu$ W/(m<sup>2</sup>/s<sup>4</sup>) at 60Hz and 400k $\Omega$  resistive load. The averaged power output at 1g is found out to be as high as 2.2mW at 60Hz resonance frequency. Based on the results obtained and AMEH capabilities to fulfil a range of power devices from wireless sensors up to communication peripherals, the mathematical model is now validated and AMEH is deemed a feasible design.

## REFERENCES

- [1] K. Cook-Chennault, "Powering MEMS Portable Devices-a Review of Non-Regenerative and Regenerative Power Supply Systems with Special Emphasis on Piezoelectric Energy Harvesting System." Smart Material and Structure, 2008.
- [2] A. Henry, J. Daniel, P. Gyuhae, "A Review of Power Harvesting from Vibration Using Piezoelectric Materials," The Shock and Vibration Digest, 36 (3), 2004, 197-205.
- [3] P. Riley, C. Saha, C. Johnson, "Designing a Low Cost, Electricity Generating Cooking Stove." IEEE Xplore. 29(2), 2010, pp.47-53.
- [4] A. Rogers, J. Manwell, S. Wright, "Wind Turbine Acoustic Noise," Renewable Energy Research Laboratory, 2002.
- [5] S. Horowitz, M. Sheplak, L. Cattafesta, T. Nishida, F. Liu, D. Johnson and K. Ngo, "A MEMS Acoustic Energy Harvester," J. Micromec. and Microeng., 2006, S174-S181.
- [6] R. Taylor, F. Liu, S. Horowitz, K. Ngo, T. Nishida, L. Cattafesta and M. Sheplak, "Technology Development for Electromechanical Acoustic Liners," ACTIVE 2004, Williamsburg, Virginia.
- [7] F. Liu, A. Phipps, S. Horowitz, K. Ngo, L. Cattafesta, T. Nishida and M. Sheplak, "Acoustic Energy Harvesting Using an Electromechanical Helmholtz Resonator" J. Acous. Soc. Am., 2008.
- [8] W. Wang, L. Wu, L. Chen and C. Liu, "Acoustic Energy Harvesting by Piezoelectric Curved Beams in the Cavity of a Sonic Crystal. Smart. Mat. Struc., 2010, 045016 (7pp).
- [9] H. Sodano, G. Park and J. Inman, "Estimation of Electric Charge Output for Piezoelectric Energy Harvesting," Strain J. Brit. Soc. Strain Measurement, 2004, pp.49-58.
- [10] F. Lu, H. Lee and S. Lim, "Modeling and Analysis of Micro Piezoelectric Power Generators for MEMS Application," Smart Material Structure, 2004, pp.57-63.
- [11] S. Chen, G. Wang and M. Chien, "Analytical Modeling of Piezoelectric Vibration-Induced Micro Power Generator," Mechatronics, 2006, pp.397-387.
- [12] A. Erturk and D. Inman, "On Mechanical Modelling of Cantilevered Piezoelectric Vibration Energy Harvesters," J. Intell. Mater. Syst. Struct., 2008, pp327-354.
- [13] S. Priya, "Modeling of Electric Energy Harvesting using Piezoelectric Windmill," Journal of Applied Physic Letter, 2005, 87, 184101.
- [14] G. Sebald, D. Lefeurve, and D. Guyomar, "Pyroelectric Energy Conversion: Optimization Principles," IEEE Transaction on ultrasonics, ferroelectrics and frequency control, 2008, pp.538-551.
- [15] S. K. Moore, "Printing Technology Makes Miniature Energy Harvesters, Antennas, and Fuel Cell Parts," IEEE Spectrum Online, 2008, pp.538-551.